

**Electrochemical Model OF Mild Steel Corrosion
in a Mixed H₂S/CO₂ Aqueous Environment**

Yougui Zheng, Jing Ning, Bruce Brown, Srdjan Nesic

Institute for Corrosion and Multiphase Technology
Department of Chemical and Biomolecular Engineering
Ohio University
342 W. State St.
Athens, OH 45701

ABSTRACT

The present study has been conducted to investigate the electrochemistry of mild steel corrosion in mixed H₂S/CO₂ aqueous environments and develop an electrochemical model to simulate the experimental results. The experiments were designed to determine the effect of H₂S on CO₂ corrosion for short term exposures of a few hours before any interference from iron sulfide corrosion product layers happened. Tests were conducted at different H₂S concentrations ranging from 0 to 10% in the gas phase at 0.1 MPa total pressure at pH4 and pH5 respectively. Corrosion rates were measured by linear polarization resistance (LPR) and the corrosion mechanisms were investigated by using potentiodynamic sweeps. Results showed that the presence of H₂S slowed down the charge transfer kinetics related to H₂CO₃ reduction and H₂O reduction on the metal surface. An electrochemical model was developed for a mixed H₂S/CO₂ system which was calibrated with new experimental results and compared to data found in the open literature. The model predictions fit experimental data well for short exposures (measured in hours) but overestimate the experimental results for longer term exposures (measured by days and weeks) due to the formation of an iron sulfide corrosion product layer, which is not accounted for in the present model.

Key words: hydrogen sulfide, carbon dioxide, electrochemistry, model.

INTRODUCTION

The corrosion in mixed carbon dioxide/hydrogen sulfide environment is an important issue in the oil and gas industry. More attention has been focused on this type of corrosion because of harsher environments encountered when exploring new sources of oil and gas, which often contain H₂S. However, little progress has been made in defining the corrosion mechanisms involved. The understanding, prediction, and control of H₂S corrosion are some of the key challenges for oil and gas production.

The severity of corrosion depends on multiple factors including temperature, pH, partial pressures of CO₂ and H₂S, and flow conditions, to name the most important ones. Therefore, there is a need for models that would predict corrosion rates under various conditions and, thus, save the cost of performing numerous experiments.

Models for CO₂ corrosion have been developed in the past, taking form of semi-empirical correlations or mechanistic models describing the different processes involved in CO₂ corrosion of carbon steel¹. In the case of H₂S corrosion, there are numerous experimental studies²⁻⁵, however, only a few models have been developed and published in the open literature for H₂S or mixed CO₂/H₂S corrosion^{6,7}.

Anderko and Young⁶ (1999) presented a mechanistic model to simulate the corrosion rates of carbon steel in a mixed CO₂/H₂S environment. The model consists of a thermodynamic part used to predict corrosion product layer composition and an electrochemical model to simulate the rate of cathodic and anodic processes on the metal surface. However, the electrochemical model was simplistically correlated to final steady state corrosion rate data to obtain a good agreement, by using a surface coverage effect by iron sulfide. No mechanistic verification of this approach was done with electrochemical kinetic data, and the steel surface water chemistry was not distinguished from bulk water chemistry, in their model.

Sun and Nestic⁷ (2010) published a mechanistic model based on a mass transfer control mechanism for corrosion in the presence of iron sulfide layers, often seen in H₂S corrosion. This mechanistic model was calibrated to fit a broad range of experimental results and was found to be useful for prediction of transient corrosion rates arising from growth of iron sulfide layers. However, the model includes a number of assumptions which were not explicitly verified. For example it was universally assumed in the model that mass transfer limits the rate of H₂S corrosion and therefore the electrochemical processes were not defined or included. This is clearly a simplification and limitation of the model which needed improvement.

In the first author's previous research⁸, an electrochemical model of carbon steel corrosion in H₂S system had been developed and verified with electrochemical kinetics experiments. It accounts for the effect of pH₂S, flow rate, pH and temperature on H₂S corrosion. An additional cathodic reaction, direct H₂S reduction, was identified and included in the model. However, in reality CO₂ is ubiquitous, so it is of key importance to extend this electrochemical model to cover mixed H₂S/CO₂ systems and include validation by more literature data. The results of this work are presented below.

EXPERIMENTAL

Equipment

Experiments were performed at atmospheric pressure in a 2 liter glass cell with 1wt% NaCl in deionized water solution. Gas (mixture of hydrogen sulfide, H₂S and carbon dioxide, CO₂) was sparged through the cell continuously. A typical three-electrode setup was used. The working electrode (WE) was a rotating cylinder electrode (RCE) made of mild steel with a speed controller. The counter electrode (CE) was a concentric ring made of platinum wire. The reference electrode (RE) was a saturated silver-silver chloride (Ag/AgCl) electrode connected to the cell externally *via* a Luggin capillary. The pH was monitored with an electrode immersed in the electrolyte. The concentration of H₂S was adjusted by a gas rotameter and measured by a gas sample pump with H₂S detector tubes. A carbon scrubber was used to treat the gas coming out of glass cell to remove the H₂S.

Material

X65 pipeline steel was used in the present experiments with a composition (as reported by the manufacturer) shown in Table 1. The WE was machined out from the parent steel material and had a diameter of 1.20 cm and a working surface area of 5.4 cm².

Table 1
Chemical composition of X65 used in RCE (wt%)

Cr	Mo	S	V	Si	C	Fe	Ni	Mn	P
0.14	0.16	0.009	0.047	0.26	0.13	Balance	0.36	1.16	0.009

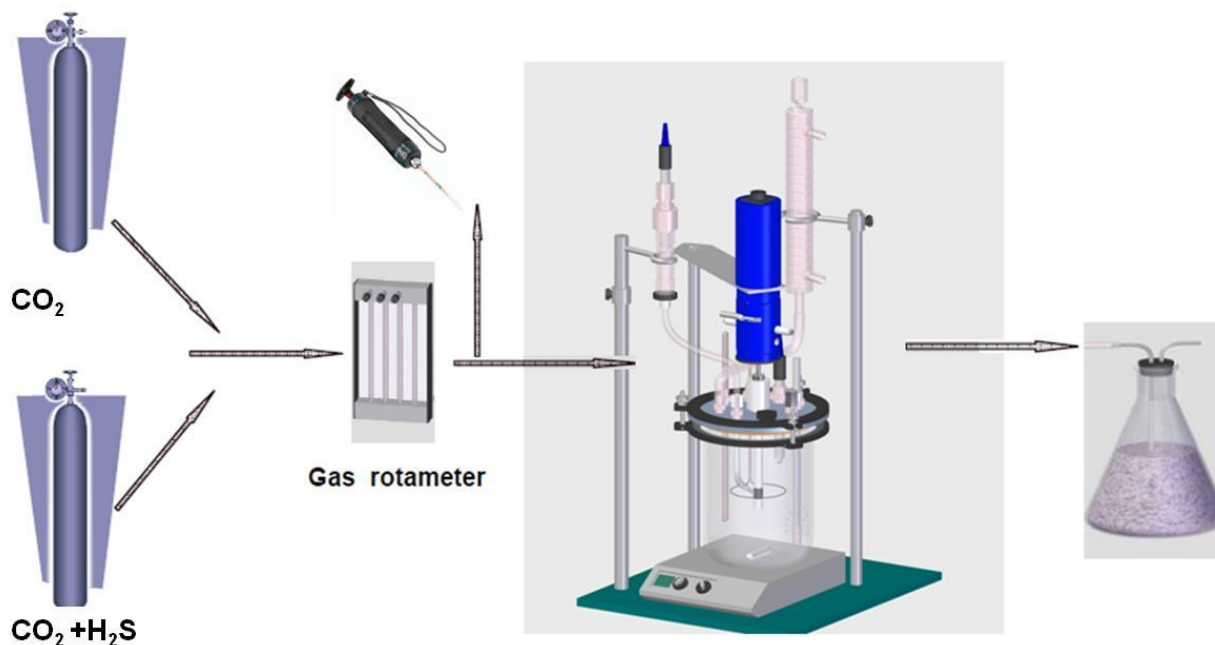


Figure 1: Schematic of the experimental set-up.

Procedure

The aqueous solution was initially deoxygenated by continuously purging CO₂ gas for at least three hours. At the same time, the solution was heated to desired temperature. After the solution was deoxygenated, H₂S was added to the purge for at least a half hour to saturate the solution at the required partial pressure of H₂S. The gas concentration was adjusted by purging different ratios of CO₂ to H₂S, from 100 ppm to 10% H₂S, corresponding respectively to a H₂S partial pressure $p_{H_2S} = 10$ Pa and 9.65 kPa, at 30°C. The pH was adjusted by adding deoxygenated hydrochloric acid or sodium hydroxide. Prior to immersion, the cylindrical mild steel specimen surfaces were polished with 400 and 600 grit sandpaper sequentially (including simultaneously cooling by isopropyl alcohol), then was washed with isopropyl propanol in an ultrasonic cleaner, and dried with an air blower.

A potentiostat was used to perform electrochemical measurements during the test. The open circuit potential (OCP) was monitored and polarization resistance (R_p) measurements were conducted by polarizing the WE ± 5 mV from the free corrosion potential and scanning at 0.125 mV/s. Solution resistance was measured independently using electrochemical impedance spectroscopy (EIS), and the measured R_p was then corrected. Corrosion rate (CR) was calculated based on measured R_p using the LPR constant $B = 23$ mV/decade. EIS measurements were carried out by applying an oscillating

potential ± 5 mV around OCP of the WE, using the frequency range 3 mHz to 5kHz. At the end of each experiment, the potentiodynamic sweeps were conducted at a sweep rate of 1 mV/s. The solution resistance was manually corrected for after the measurements. The test matrix for the experimental work is shown in Table 2.

Table 2
Test Matrix.

Description	Parameters
Test Material	X65
Test Solution	1 wt% NaCl Solution
Purged Gas(H ₂ S volume fraction in H ₂ S/CO ₂)	0 -10%(v) (0 -0.01Mpa)
Rotating Speed / rpm	1000
Total Pressure / MPa	0.1
Temperature /°C	30
pH	4, 5
Test Duration/ hour	0.5 to 2
Measurement Methods	LPR, EIS, Potentiodynamic Sweeps

RESULTS AND DISCUSSION

Effect of pH₂S

Table 3 shows the unit conversion of ppm (part per million) to Pa for H₂S concentration in gas phase. The unit of ppm or % used here is based on a volume fraction (volume H₂S in the total mixture H₂S/CO₂ gas). Only the dry gas mixture of H₂S and CO₂ without water vapor was measured before purging into glass cell system. There is always some water vapor in the gas phase of any system containing water. When converting ppm or % to partial pressure of H₂S, the water vapor pressure needs to be considered, especially in high temperature environments.

Table 3
The unit conversion of ppm or % to kPa for H₂S in gas phase
at 30°C, 0.1 MPa total pressure

H ₂ S volume fraction in the total mixture H ₂ S/CO ₂ gas	100ppm	500ppm	0.65%	6%	10%
H ₂ S partial pressure / kPa	0.01	0.05	0.63	5.82	9.65

Corrosion rates at different H₂S concentrations in the H₂S/CO₂ mixture, pH4, and 1000 rpm rotating speed condition are shown in Figure 2. The corrosion rate under a pure CO₂ environment (zero H₂S concentration) at pH4 was about 2.7 mm/year. When H₂S gas concentration was increased to 100 ppm and 500 ppm, the corrosion rates were reduced to 1.4 and 1.5 mm/year and then increased again to 2.4 mm/year at 10% H₂S gas concentration. Similar behavior was observed at pH 5 (Figure 3).

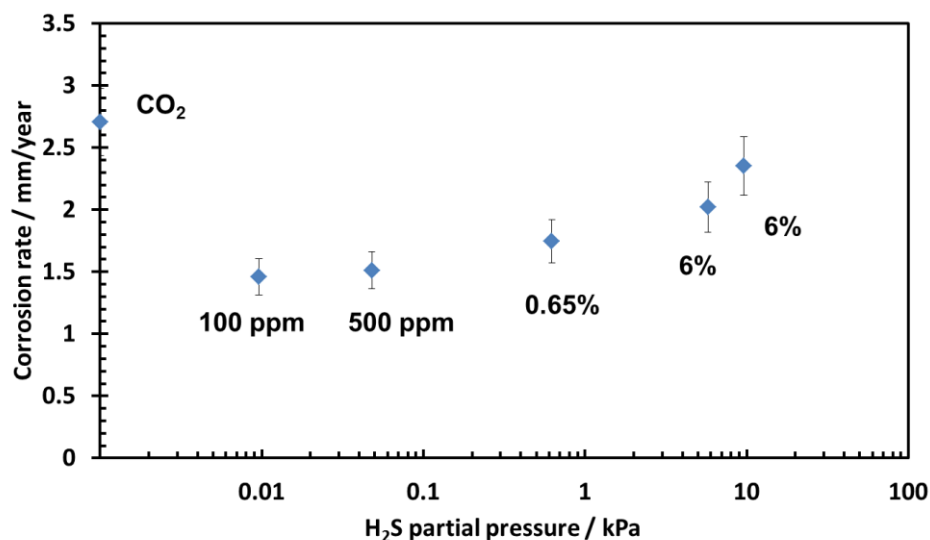


Figure 2: Effect of H₂S gas concentration in the H₂S/CO₂ mixture at total pressure 0.1 Mpa, on corrosion rates of mild steel at pH4, 30°C, 1wt% NaCl, 1000 rpm rotating speed, exposure time < 2 hours, B = 23 mV/ decade.

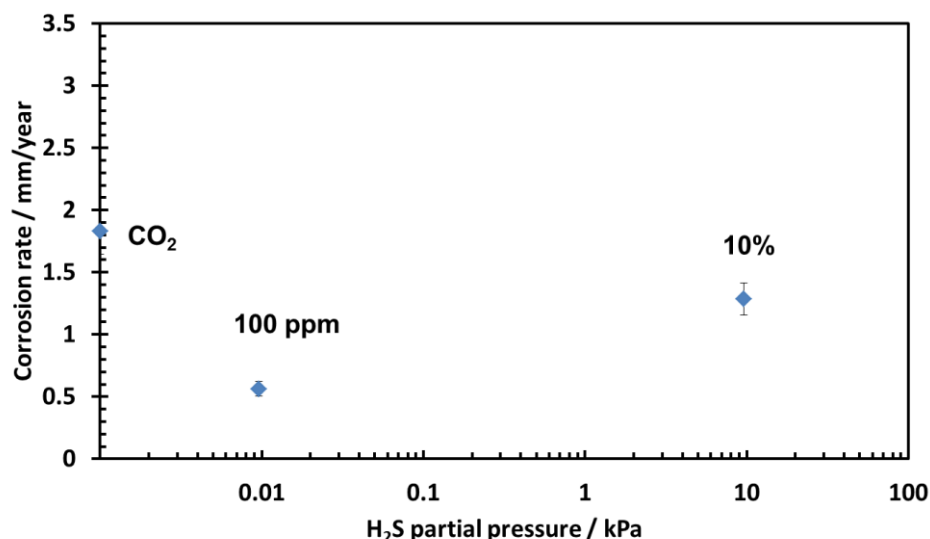
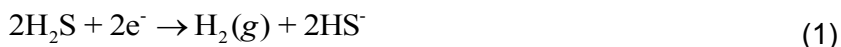


Figure 3: Effect of H₂S gas concentration in the H₂S/CO₂ mixture at total pressure of 0.1 Mpa, on corrosion rates of mild steel at pH5, 30°C, 1wt% NaCl, 1000rpm rotating speed, exposure time < 2 hours, B = 23 mV/ decade

The effect of H₂S on cathodic potentiodynamic sweeps at pH4 and pH5 are shown in Figure 4 and Figure 5. At pH4, the cathodic polarization curve in a pure CO₂ aqueous environment (without any H₂S) has the same shape as previously reported by others⁹. It shows a limiting cathodic current region in the range -720 mV to -900 mV, which consists of the diffusion limited current of H⁺ reduction and chemical reaction controlled current of H₂CO₃ reduction. At a more negative potential a charge transfer current region is seen corresponding to direct H₂O reduction. When 100 ppm or 500 ppm H₂S was introduced, the mass transfer limiting current did not change compared with a pure CO₂ purged environment, but the H₂O reduction rate was slowed down; this agreed with the observation reported previously for a H₂S environment (without CO₂)⁸. As the H₂S gas concentration increased (to 0.65% and higher to 10%), the cathodic limiting current plateau moved to higher currents and a second "wave" in the limiting current at

more cathodic potential also appeared, which is due to the direct reduction of H₂S on the steel surface⁸ according to:



At pH5, the same trend was observed. The mass transfer limiting current did not change at 100 ppm H₂S, but increased at 10% H₂S. The water reduction rate was retarded at pH5, as well.

The effect of H₂S concentration on the anodic iron dissolution reaction at pH4 and pH5 can also be seen in the potentiodynamic sweeps (Figure 4 and Figure 5). At pH4 (Figure 4), with 100 ppm and 1000 ppm H₂S, the anodic potentiodynamic sweeps shifted to lower currents as compared with a pure CO₂ environment, which indicates a retardation effect due to H₂S. As H₂S gas concentration increased up to 6% and 10% in the H₂S/CO₂ mixture, the anodic reaction rate increased, and eventually reached the same rate as in a pure CO₂ environment. At pH5 (Figure 5), the similar behavior of the anodic potentiodynamic sweeps was observed. As previously reported⁸, this is related to HS⁻ adsorption on the steel surface which has a catalytic effect.

To summarize the experimental findings, the presence of H₂S in a CO₂ dominated aqueous environment affects both the cathodic and anodic reactions, and may lead to either acceleration or retardation of corrosion rate of the steel, depending on H₂S concentration. A new cathodic reaction is direct reduction of H₂S. The H₂O reduction rate is slowed down in the presence of the H₂S. The effect of H₂S on the charge transfer kinetics of H₂CO₃ reduction is not as clear from the potentiodynamic sweeps because of the interference by the iron dissolution anodic reaction and the mass transfer limiting current. However, based on the corrosion rate measurements, it appears that H₂CO₃ reduction is also slowed down in the presence of the H₂S, making it similar what was observed for H₂O reduction. For the anodic reaction, the same phenomena was observed as seen in pure H₂S environments⁸, which is dependent primarily on H₂S concentration.

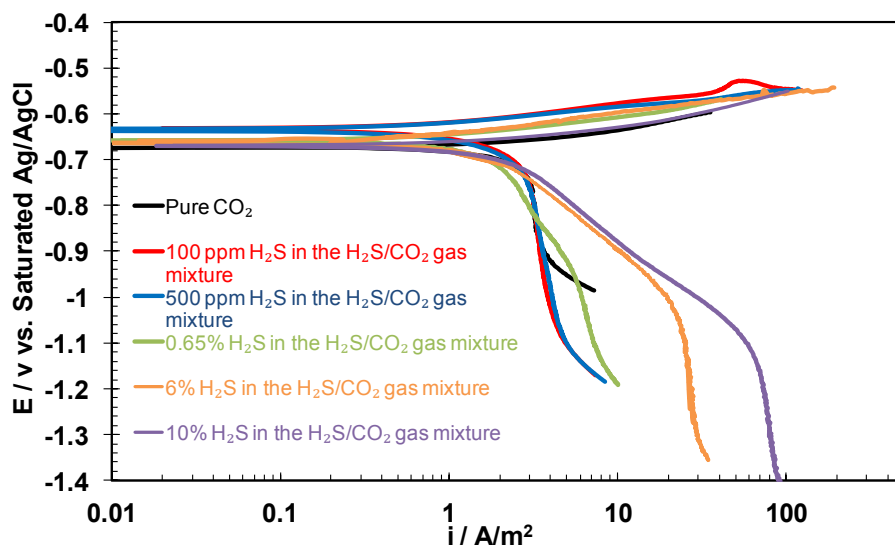


Figure 4: Effect of H₂S gas concentration in the H₂S/CO₂ mixture at total pressure 0.1 Mpa on potentiodynamic sweeps of mild steel corrosion at pH4, 30°C, 1wt% NaCl, 1000rpm rotating speed, exposure time < 2 hours

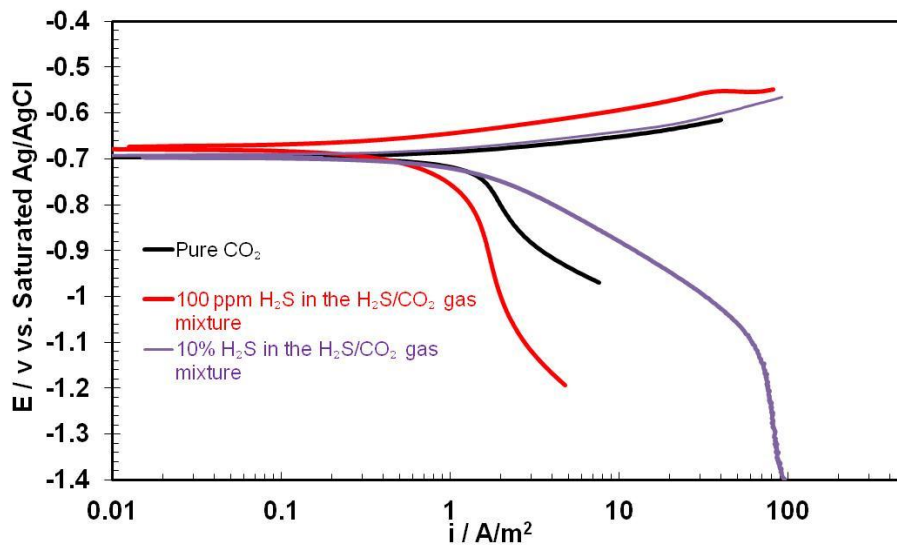


Figure 5: Effect of H₂S gas concentration in the H₂S/CO₂ mixture at total pressure 0.1 Mpa on potentiodynamic sweeps of mild steel corrosion at pH5, 30°C, 1wt% NaCl, 1000rpm rotating speed, exposure time < 2 hours

Effect of pH

Solution without H₂S

The effect of pH in aqueous solutions saturated with CO₂ (without any H₂S) on potentiodynamic sweeps is shown in Figure 6. The change of pH from pH4 to pH5 agrees with the previous findings of Nestic, *et al.*⁹ The limiting current density decreased by a factor 2-3, and not 10, because of the contribution from a chemical reaction-limited H₂CO₃ reduction. Figure 6 also shows pH had a very small effect on the anodic reaction from pH4 to pH5.

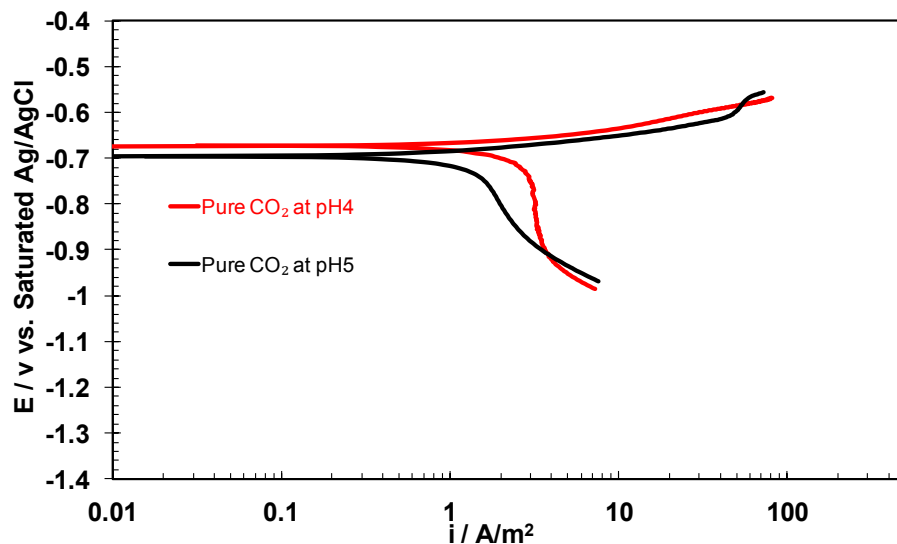


Figure 6. Effect of pH on potentiodynamic sweeps of mild steel corrosion in the solution purged with pure CO₂ at 30°C, total pressure of 0.1Mpa, 1wt% NaCl, 1000rpm rotating speed, exposure time < 2 hours.

Solution with H₂S

The change of the potentiodynamic sweeps from pH4 to pH5 in an aqueous solution purged with 100ppm H₂S in the gas mixture (Figure 7) has the same trend as that in a pure CO₂ purged solution for both cathodic and anodic parts.

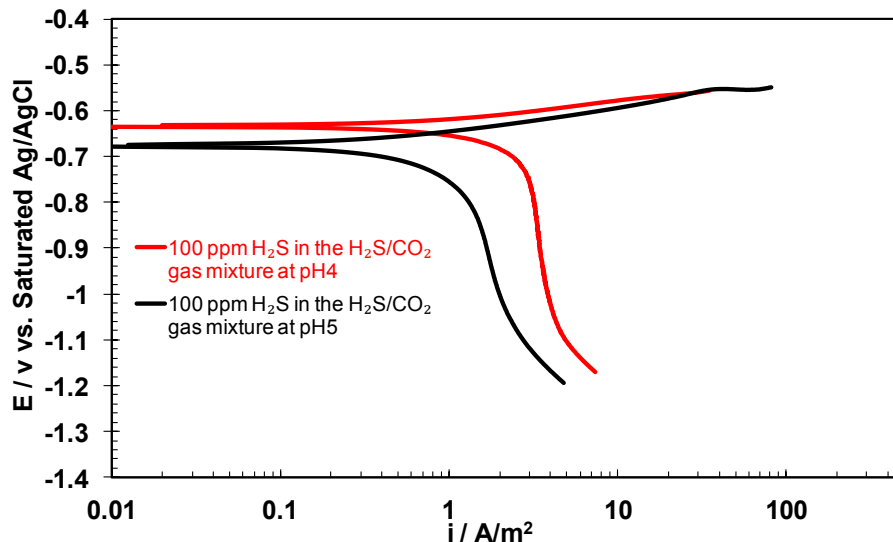


Figure 7: Effect of pH on potentiodynamic sweeps of mild steel corrosion in the solution purged with 100 ppm H₂S in the H₂S /CO₂ gas mixture at total pressure of 0.1Mpa, 30°C, 1wt% NaCl, 1000rpm rotating speed, exposure time < 2 hours.

When H₂S concentration increased to 10%, the effect of pH on potentiodynamic sweeps is shown in Figure 8. The limiting current was almost the same at pH4 and pH5, which is different behavior from a three-fold change in pH seen in a “CO₂ only” environment. The reason is that the main contribution to the cathodic limiting current at 10% H₂S concentration is from the aqueous H₂S species, whose concentration is independent of pH.

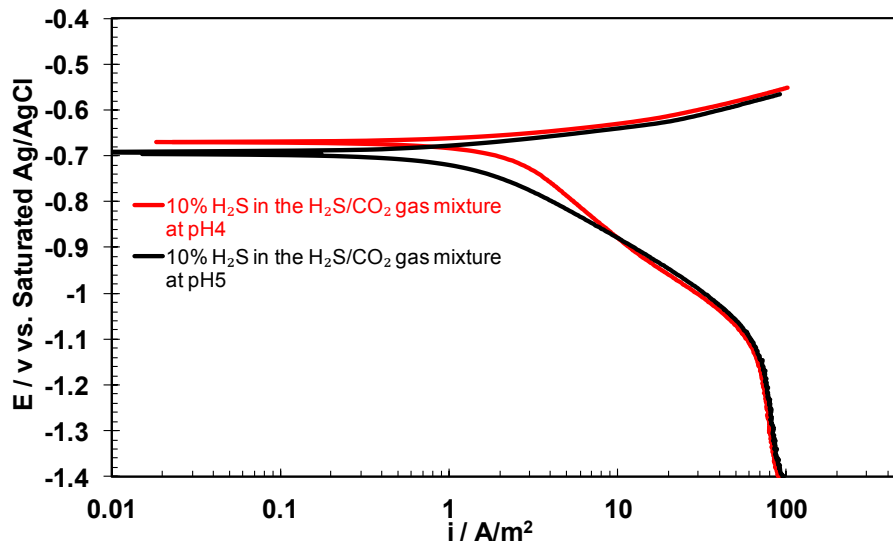


Figure 8: Effect of pH on potentiodynamic sweeps of mild steel corrosion in the solution purged with 10% H₂S in the H₂S /CO₂ gas mixture at total pressure of 0.1Mpa, 30°C, 1wt% NaCl, 1000rpm rotating speed, exposure time < 2 hours.

Both Figure 7 and Figure 8 show that pH had a smaller effect on the anodic dissolution reaction in the range of conditions studied.

ELECTROCHEMICAL MODEL

Anodic Reaction

The only anodic reaction is iron dissolution from the steel surface:



The detailed model of iron dissolution in CO₂ environment without H₂S has been reported by Nescic et al.⁹ This reaction is under charge transfer control. Thus, pure Tafel behavior can be assumed close to the corrosion potential.

$$i_{Fe} = i_{0,Fe} \times 10^{\frac{\eta}{b_a}} \quad (3)$$

The reference exchange current density $i_{0,Fe}^*$ at room temperature, 293.15K is 1 A/m² for X-65 steel. The activation energy ΔH was found to be 37.5 kJ/mol. The Tafel slope is $b_a = \frac{2.303RT}{1.5F}$. The reversible potential of X-65 steel was taken⁹ to be – 0.488 V.

When H₂S is present, the anodic reaction rate is observed to mostly depend on H₂S concentration, as shown in Figure 4 and Figure 5,. This behavior is modeled as proposed in the previous study⁸, where the exchange current density is related to the surface coverage by HS⁻ ions(θ_{HS^-}) and follows the Langmuir adsorption model.

$$i_{0,Fe} = i_{0,Fe}^* \theta_{HS^-} e^{\frac{\Delta H}{R} \left(\frac{1}{T} - \frac{1}{T_{ref}} \right)} \quad (4)$$

$$\theta_{HS^-} = \frac{K_2 C_{HS^-}}{1 + K_2 C_{HS^-}} \quad (5)$$

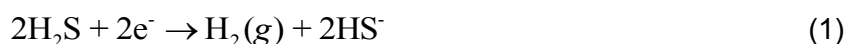
Cathodic Reactions

In the model, there are four cathodic reactions in a mixed CO₂/H₂S aqueous system:

- reduction of H⁺ ions:



- direct reduction of aqueous H₂S (as described in the previous study⁸):



- direct H₂CO₃ reduction:



- direct H₂O reduction:



The details of H⁺ reduction, H₂S reduction, H₂O reduction have been described in the previous paper⁸ which covers these same reactions for a pure H₂S system, and no change is made in the present work for a mixed CO₂/H₂S aqueous system. However modeling of H₂CO₃ reduction with and without H₂S is done differently and will be addressed below.

Modeling of H₂CO₃ reduction for a pure CO₂ aqueous system (without H₂S) has been described clearly by Nescic et al.⁹ The total current density of H₂CO₃ reduction is given by:

$$\frac{1}{i_{\text{H}_2\text{CO}_3}} = \frac{1}{i_{\alpha, \text{H}_2\text{CO}_3}} + \frac{1}{i_{\text{lim}, \text{H}_2\text{CO}_3}^r} \quad (9)$$

where $i_{\text{H}_2\text{CO}_3}$, $i_{\alpha, \text{H}_2\text{CO}_3}$ and $i_{\text{lim}, \text{H}_2\text{CO}_3}^r$ are the total current density, the charge transfer current density and the mass transfer limiting current density of this reaction in A/m², respectively.

Charge transfer current density of this reaction can be calculated using the equation:

$$i_{\alpha, \text{H}_2\text{CO}_3} = i_{0, \text{H}_2\text{CO}_3} \times 10^{\frac{-\eta}{b_c}} \quad (10)$$

Tafel slope and reversible potential can be calculated from Equation (11) and (12)

$$b_c = \frac{2.303RT}{\alpha_c F} \quad (11)$$

$$E_{\text{rev}} = -\frac{2.303RT}{F} \text{pH} - \frac{2.303RT}{2F} \log P_{\text{H}_2} \quad (12)$$

$\alpha_c = 0.5$ giving $b_c \approx 0.120$ V/decade at 30°C, and the P_{H_2} is set to 1 bar (0.1 Mpa).

The exchange current density can be calculated by:

$$i_{0, \text{H}_2\text{CO}_3} = i_0^{\text{ref}} \left(\frac{C_{\text{H}_2\text{CO}_3}}{C_{\text{H}_2\text{CO}_3 \text{ref}}} \right)^{0.5} \left(\frac{C_{\text{H}^+}}{C_{\text{H}^+ \text{ref}}} \right)^{-0.5} \times e^{\frac{\Delta H}{R} \left(\frac{1}{T} - \frac{1}{T_{\text{ref}}} \right)} \quad (13)$$

From Nescic^{9, 10}, the $i_{0 \text{ref}}$ for H₂CO₃ reduction was taken to be 0.018 A/m² at 293.15K reference temperature and 1×10⁻⁴ mol/L reference H₂CO₃ concentration. The enthalpy of activation in Equation (5) is set to 50 kJ/mol.⁹

The CO₂ hydration reaction limiting current density can be calculated using⁹:

$$i_{\text{lim}(H_2CO_3)}^r = f \times F[CO_2]_b \times (D_{H_2CO_3} K_{hyd} K_{hyd}^f)^{0.5} \quad (14)$$

where $[CO_2]_b$ is the bulk concentration of dissolved carbon dioxide, which can be obtained from:

$$[CO_2]_b = k_{CO_2}^d \times P_{CO_2} \quad (15)$$

Henry's constant $k_{CO_2}^d$ as a function of temperature can be calculated using¹⁰:

$$k_{CO_2}^d = 14.5 / 1.00258 \times 10^{-(2.27 + 5.65 \times 10^{-3} T_f - 8.06 \times 10^{-6} T_f^2 + 0.075 \times I)} \quad (16)$$

The equilibrium constant for the CO_2 hydration reaction, K_{hyd} , is equal to 2.58×10^{-3} and does not change with temperature¹⁰. The forward hydration reaction constant (k_{hyd}^f) is a function of temperature, which is given as¹⁰:

$$k_{hyd}^f = 10^{32985 - 11054 \log T_k - \frac{172654}{T_k}} \quad (17)$$

From experimental observation, it was found that when H_2S was present, the H_2O reduction rate was slowed down by approximately 1 or 2 orders of magnitude. Similarly, it is considered here that H_2CO_3 reduction was also slowed down due to the presence of H_2S . In an H_2S environment, the i_0^{ref} for H_2CO_3 reduction was taken to be 0.006 A/m^2 (3 times lower than the 0.018 A/m^2 used for a pure CO_2 environment without H_2S). The other parameters were taken to be the same as in the model without H_2S .

Implementation of the Model

The model requires as input: temperature, pH, P_{H_2S} , P_{CO_2} and the hydrodynamic parameters, in this case, the rotating cylinder diameter, and the rotational velocity. The corrosion potential then can be calculated by solving the charge balance equation:

$$\sum i_a = \sum i_c \quad (18)$$

which here takes the form:

$$i_{Fe} = i_{H_2CO_3} + i_{H_2S} + i_{H^+} + i_{H_2O} \quad (19)$$

Once the corrosion potential is found, the corrosion current and rate can be found from the anodic current (or total cathodic current) at the corrosion potential. The individual and total cathodic and anodic curves and predicted potentiodynamic sweeps can be generated.

MODEL VALIDATION

Performance of the model was validated by comparing the calculations with experimental results described above and with external data obtained from the open literature.

Comparison with results from the present experimental study

First, the electrochemical model in pure CO₂ environment without H₂S is validated with the experimental results at pH4 and pH5. Figure 9 and Figure 10 show the comparison of the potentiodynamic sweeps simulated by the model with experimental data. It can be seen that the potentiodynamic sweeps capture the corrosion processes very well and the calculated results are in a very good agreement with all experimental results.

Second, the effect of H₂S addition was simulated with the electrochemical model. Figure 11 and Figure 12 show the comparisons of simulated sweeps with experimental results at pH4. Model simulations capture cathodic and anodic potentiodynamic sweeps changes with increasing H₂S gas concentration and generally agree with experimental potentiodynamic sweeps at the different H₂S concentration. Figure 13 and Figure 14 show the corrosion rates calculated by the electrochemical model are in good agreement with experimental results, which all suggests that the electrochemical model captures the main electrochemical processes underlying H₂S/CO₂ corrosion.

Comparison with results of external experimental studies

The electrochemical model was also validated with external data obtained from the open literature. Model performance was examined first in low partial pressure of H₂S (pH₂S ranged from 55 Pa to 330 Pa, corresponding to 55 ppm to 340 ppm in the gas phase at 0.1 MPa CO₂), where the experiments were conducted by Lee.¹¹ Figure 15 shows the corrosion rates change with H₂S partial pressure. It shows even a very low concentration of H₂S (50 ppm or 5 Pa) can reduce the CO₂ corrosion rate which is greater than 1 mm/y in absence of H₂S. The model captures this effect clearly.

Corrosion experiments at a somewhat higher concentration of H₂S (pH₂S ranging from 0.1 kPa to 0.98 kPa, corresponding to 1000 ppm to 10,000 ppm H₂S in the mixed H₂S /CO₂ gas phase) was reported by Choi¹². Model prediction are compared with the experimental results in Figure 16. Corrosion rates do not change much with H₂S concentration from 0.1 kPa to 0.98 kPa, which is broadly captured by the model.

The effect of temperature on corrosion rate was investigated by Abayarathna et al.¹³ where corrosion rates increased with temperature at different H₂S concentration conditions. The experiments were simulated using the present CO₂/H₂S model and it was found that the model can predict the measured corrosion rate change, as shown in Figure 17.

A corrosion case at more severe conditions was reported by Bich et al.¹⁴ The experimental condition includes high partial pressures of CO₂ (pCO₂ = 0.3 MPa to 1.28 MPa) and H₂S (pH₂S = 0.3 MPa to 2.0 MPa). The predicted corrosion rates are within a factor of 2 of the measured data points as Figure 18 shows.

Long-term flow loop experiments (15 – 21 days) at high partial pressure of H₂S (pH₂S = 1.0 MPa to 3.0 MPa), high partial pressure of CO₂ (pCO₂ = 0.33 MPa to 1.0 MPa) was conducted by Omar, et al.¹⁵ Figure 19 shows comparison between present electrochemical model prediction and experimental results. The model over-predicts the corrosion rate by a large factor of 10 to 50. This is due to the formation of iron sulfide layers on the surface, which are not accounted for in the current model. Sun and Netic's model⁷ considers the effect of iron sulfide corrosion product layers and makes a better

prediction for long term experiments, as Figure 20⁷ shows. Further extension of the current electrochemical model to include mass transfer effects due to iron sulfide layer formation, such as was done by Sun's and Nescic⁷, is ongoing.

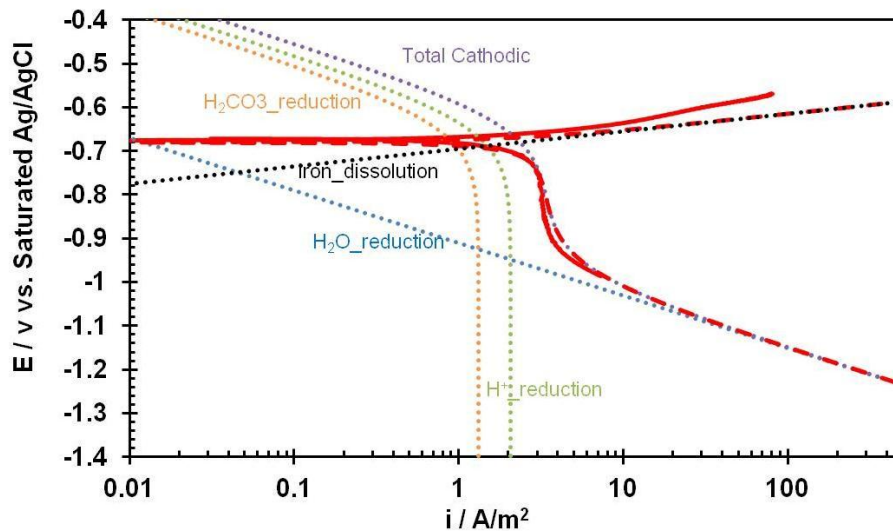


Figure 9: Comparison between predicted potentiodynamic sweeps and experimental results in the solution purged with pure CO₂ at pH4, 30°C, total pressure of 0.1 MPa, 1wt% NaCl, 1000rpm rotating speed, exposure time < 2 hours.

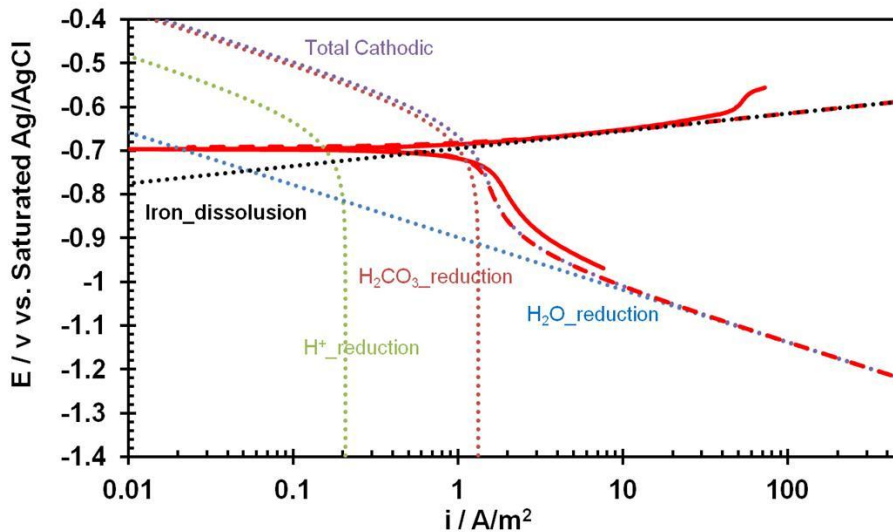


Figure 10: Comparison between predicted potentiodynamic sweeps and experimental results in the solution purged with pure CO₂ at pH5, 30°C, total pressure of 0.1 MPa, 1wt% NaCl, 1000rpm rotating speed, exposure time < 2 hours.

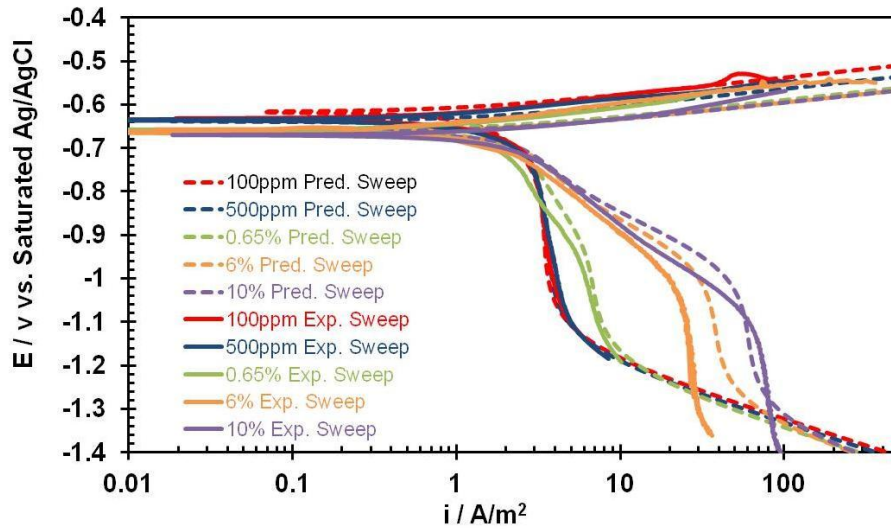


Figure 11: Comparison of predicted potentiodynamic sweeps with experimental results in the solution purged with different H_2S gas concentrations in the H_2S/CO_2 gas mixture at pH4, 30°C, total pressure of 0.1 MPa, 1wt% NaCl, 1000rpm rotating speed, exposure time < 2 hours.

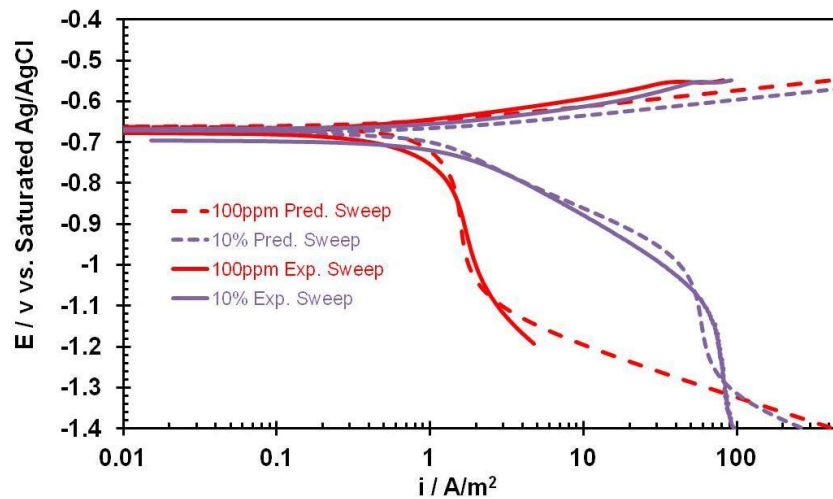


Figure 12: Comparison of predicted potentiodynamic sweeps with experimental results in the solution purged with different H_2S gas concentrations in the H_2S/CO_2 gas mixture at pH5, 30°C, total pressure of 0.1 MPa, 1wt% NaCl, 1000rpm rotating speed, exposure time < 2 hours.

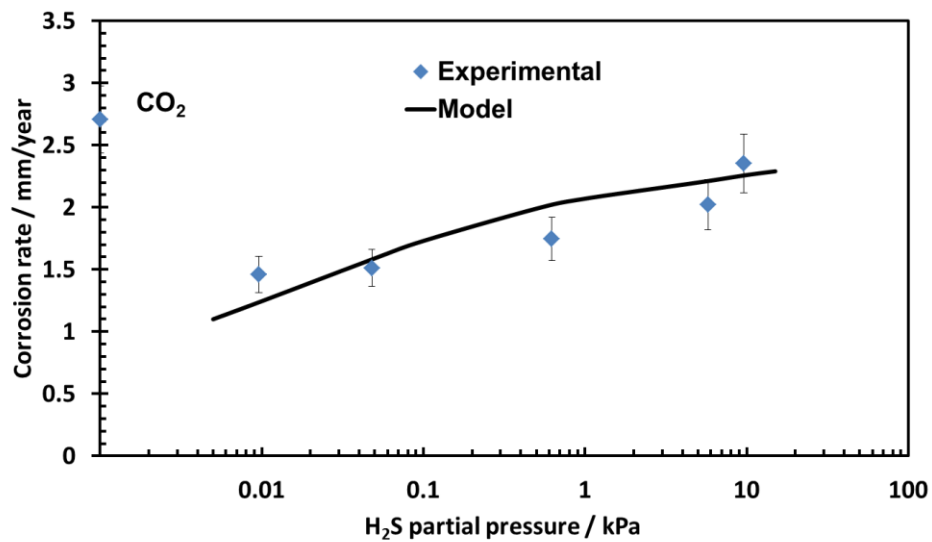


Figure 13: Comparison of corrosion rate predictions with experimental results in the solution purged with different H₂S gas concentrations in the H₂S/CO₂ gas mixture at pH4, 30°C, total pressure of 0.1 MPa, 1wt% NaCl, 1000rpm rotating speed, exposure time < 2 hours.

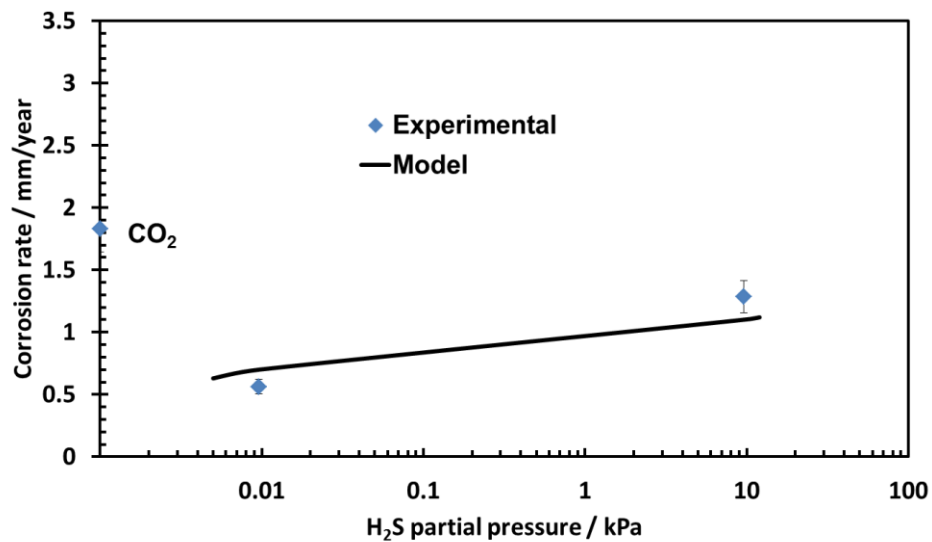


Figure 14: Comparison of corrosion rate predictions with experimental results in the solution purged with different H₂S gas concentrations in the H₂S/CO₂ gas mixture at pH4, 30°C, total pressure of 0.1 MPa, 1wt% NaCl, 1000rpm rotating speed, exposure time < 2 hours.

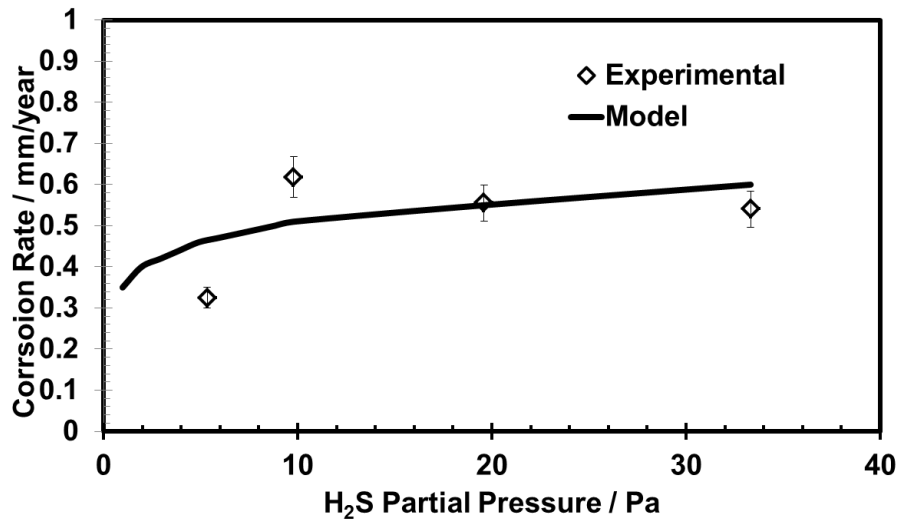


Figure 15: Comparison of corrosion rate predictions with experimental results in the solution purged with different partial pressures of H₂S gas in the H₂S/CO₂ gas mixture at total pressure of 0.1 MPa, at pH5, 20°C, 1wt% NaCl, 1000 rpm, exposure time <1 h. Data taken from Lee¹¹.

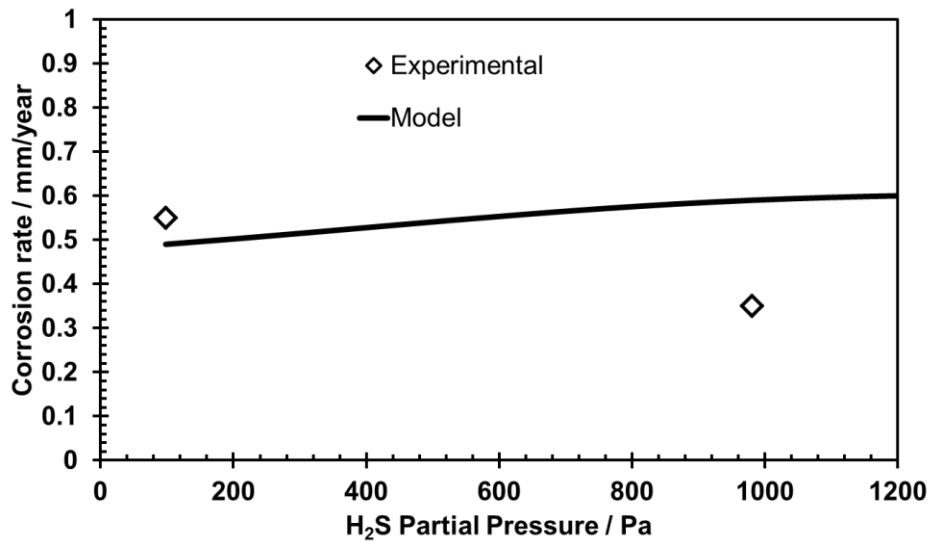


Figure 16: Comparison of corrosion rate predictions with experimental results in the solution purged with different partial pressures of H₂S gas in the H₂S/CO₂ gas mixture at total pressure of 0.1 MPa, at pH4, 25°C, 1wt% NaCl, stagnant solution (0.01 m/s used in model), exposure time <1 hour. Data taken from Choi et al.¹²

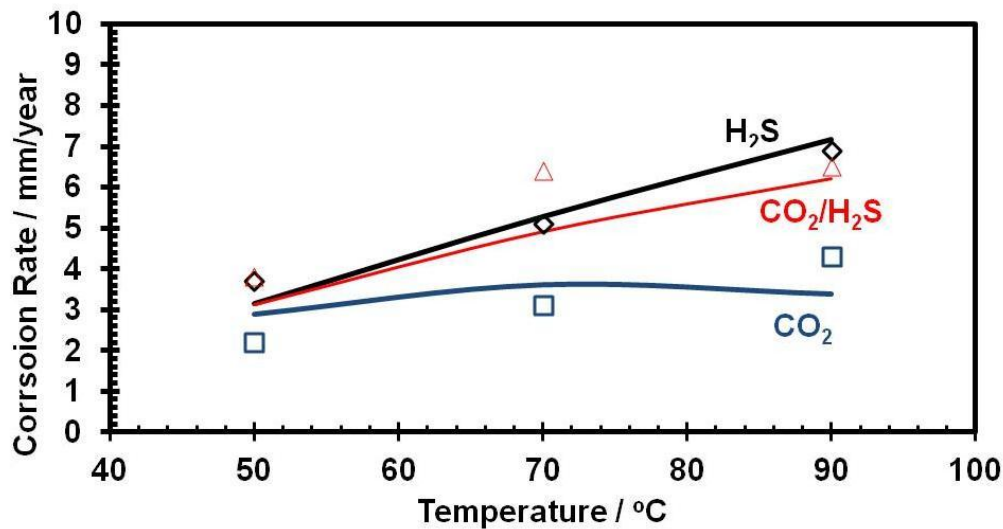


Figure 17: Comparison of corrosion rate predictions with experimental results for different temperatures; experimental data shown as points, model predictions shown as lines; total pressure = 0.1 MPa, exposure <1 hour, pH4.2 (4.5 at 90°C, CO₂), stirring condition. Assumed model parameters: volume ratio for mixture CO₂/H₂S=1:1, flow velocity 0.3 m/s. Data taken from Abayarathna et al.¹³

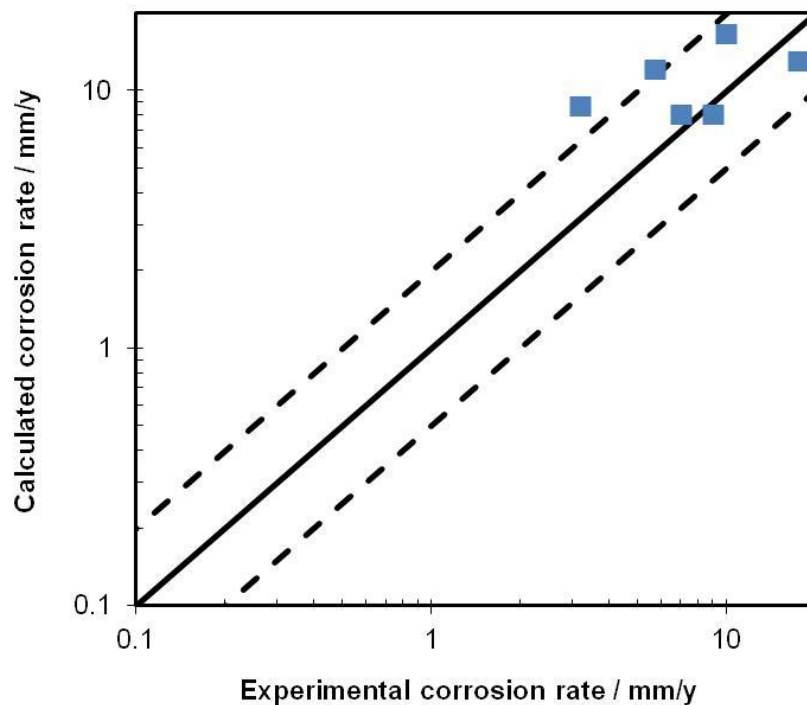


Figure 18: Parity plot showing a direct comparison of predicted and experimental corrosion rates; data taken from Bich and Goerz.¹⁴ pCO₂ = 0.3 MPa to 1.28 MPa, pH₂S = 0.3 MPa to 1.22 MPa, pH 5.0, v = 0.1 m/s. The solid line represents perfect agreement of experimental and calculated corrosion rates. The dashed lines represent a factor of 2 deviation.

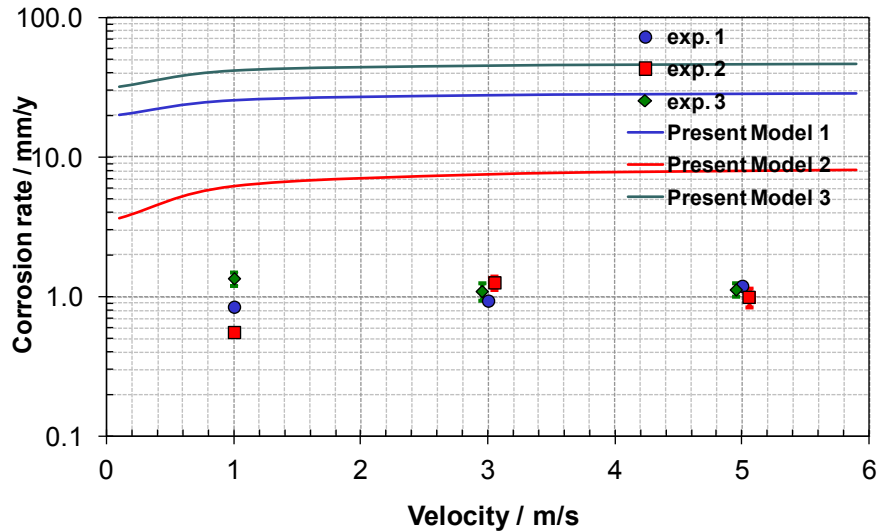


Figure 19: Comparison of corrosion rate predictions with experimental results for different velocities; experimental data shown as points, present electrochemical model predictions shown as lines; exp. 1: 19 days, $p = 4.0$ MPa, $p\text{CO}_2 = 0.33$ MPa, $p\text{H}_2\text{S} = 1.0$ MPa, 80°C , $\text{pH } 3.5$, $v = 1$ m/s to 5 m/s; exp. 2: 21 days, $p = 4.0$ MPa, $p\text{CO}_2 = 0.33$ MPa, $p\text{H}_2\text{S} = 1.0$ MPa, 25°C , $\text{pH } 3.5$, $v = 1$ m/s to 5 m/s; exp. 3: 10 days, $p = 4.0$ MPa, $p\text{CO}_2 = 1.0$ Mpa, $p\text{H}_2\text{S} = 3.0$ Mpa, 80°C , $\text{pH } 3.2$, $v = 1$ m/s to 5 m/s; experimental data taken from Omar, et al.¹⁵

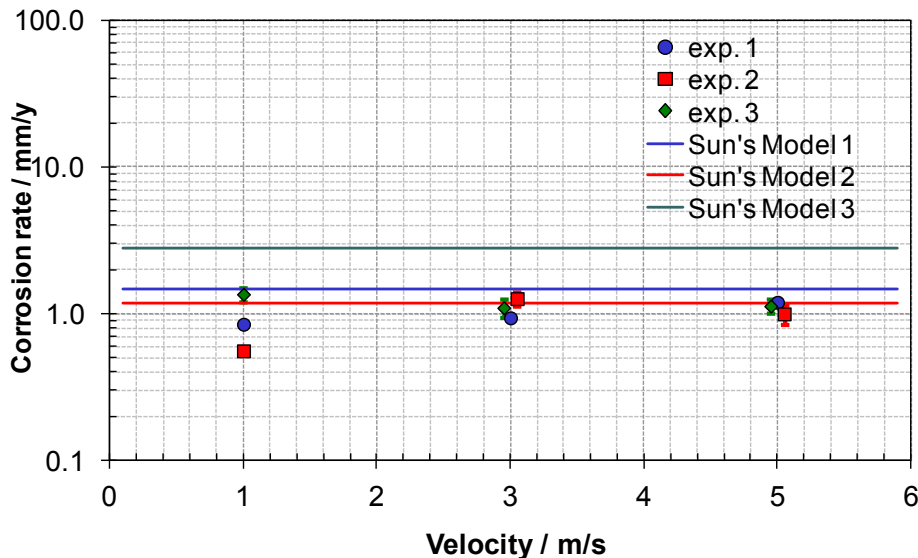


Figure 20: Comparison of corrosion rate predictions with experimental results for different velocities; experimental data shown as points, Sun and Nesci's⁷ mass transfer model predictions shown as lines; exp. 1.: 19 days, $p = 4.0$ MPa, $p\text{CO}_2 = 0.33$ MPa, $p\text{H}_2\text{S} = 1.0$ MPa, 80°C , $\text{pH } 3.5$ (calculated), $v = 1$ m/s to 5 m/s; exp. 2.: 21 days, $p = 4.0$ MPa, $p\text{CO}_2 = 0.33$ MPa, $p\text{H}_2\text{S} = 1.0$ MPa, 25°C , $\text{pH } 3.5$ (calculated), $v = 1$ m/s to 5 m/s; exp. 3.: 10 days, $p = 4.0$ MPa, $p\text{CO}_2 = 1.0$ MPa, $p\text{H}_2\text{S} = 3.0$ MPa, 80°C , $\text{pH } 3.2$ (calculated), $v = 1$ m/s to 5 m/s; experimental data taken from Omar, et al.¹⁵

CONCLUSIONS

1. A mechanistic study of H₂S corrosion kinetics for X65 steel in short term exposure was extended to include the effects seen in a mixed H₂S/CO₂ environment
2. The effect of H₂S on the anodic dissolution of iron was the same as previously observed behavior in a pure H₂S environment and included retardation or acceleration depending on the H₂S concentration.
3. An order of magnitude retardation of H₂O reduction due to the presence of H₂S was observed in all experimental conditions; it is postulated that the presence of H₂S also slows down the charge transfer kinetics of H₂CO₃ reduction approximately by a factor of 3.
4. An electrochemical model of aqueous H₂S corrosion of X65 steel was extended to cover H₂S/CO₂ saturated solutions. The model has been calibrated to fit the new experimental results and was compared with external data found in the open literature. A good agreement with the experimental data has been obtained for short term exposures where the effect of iron sulfide corrosion product layers can be ignored.

ACKNOWLEDGEMENTS

The authors would like to express sincere appreciation to the following industrial sponsors for their financial support and direction: BP, Champion Technologies, Chevron, Clariant Oil Services, ConocoPhillips, ENI S. P. A., ExxonMobil, Inpex Corporation, NALCO Energy Services, Occidental Petroleum Co., Petrobras, PETRONAS, PTT, Saudi Aramco, Total, TransCanada, MI-SWACO, HESS and WGIM.

REFERENCES

- [1] R. Nyborg, "Overview of CO₂ Corrosion Models for Wells and Pipelines", CORROSION/2002, paper no. 02233 (Houston, TX: NACE International, 2002).
- [2] S. N. Smith, J.L. Pacheco, "Prediction of Corrosion in Slightly Sour Environments", CORROSION/2002, paper no. 02241 (Houston, TX: NACE, 2002).
- [3] K.L.J. Lee, "A mechanistic modeling of CO₂ corrosion of mild steel in the presence of H₂S", (Ph. D. dissertation, Dept. Chem. Eng, Ohio University, 2004).
- [4] M. Singer, B. Brown, A. Camacho, S. Netic, "Combined Effect of CO₂, H₂S and Acetic Acid on Bottom of the Line Corrosion", CORROSION/2007, Paper no: 07661 (Houston, TX: NACE, 2007).
- [5] W. Sun, "Kinetics of iron carbonate and iron sulfide scale formation in carbon dioxide/hydrogen sulfide corrosion", (Ph.D. dissertation, Ohio University, 2006).
- [6] A.M. Anderko, R.D. Young, "Simulation of CO₂/H₂S Corrosion using Thermodynamic and Electrochemical Models", CORROSION/99, paper no. 99031 (Houston TX: NACE International, 1999).
- [7] W. Sun, S. Netic, "A Mechanistic Model of Uniform Hydrogen Sulfide/Carbon Dioxide Corrosion of Mild Steel", Corrosion 65, 5 (2009): p. 291-307.

- [8] Y. Zheng, B. Brown, S. Netic, "Electrochemical Study and Modeling of H₂S Corrosion of Mild Steel", CORROSION/2013, paper no. 2406 (Houston, TX: NACE, 2013).
- [9] S. Netic, J. Postlethwaite, S. Olsen, "An Electrochemical Model for Prediction of Corrosion of Mild Steel in Aqueous Carbon Dioxide Solutions", Corrosion 52, 04 (1996): p. 280-294.
- [10] M. Nordsveen, S. Netic, N. Nyborg, A. Stangeland, "A Mechanistic Model for Carbon Dioxide Corrosion of Mild Steel in the Presence of Protective Iron Carbonate Films Part 1: Theory and Verification", Corrosion 59, 05 (2003): p. 433-456.
- [11] K.L.J. Lee, Laboratory Notebook of Institute for Corrosion and Multiphase technology, Ohio University. Book number: 9960, APR, 2003-MAY, 2005.
- [12] Y. Choi, S. Netic, S. Ling, "Effect of H₂S on the CO₂ Corrosion of Carbon Steel in Acidic Solutions", Electrochim. Acta 56, 4 (2011): p. 1752-1760.
- [13] D. Abayarathna, A.R. Naraghi, S. Wang, "The Effect of Surface Films on Corrosion of Carbon Steel in a CO₂-H₂S-H₂O System", CORROSION/2005, Paper number: 08417 (Houston, Tx: NACE, 2005).
- [14] N.N. Bich, K.G. Goerz, "Caroline Pipeline Failure: Findings on Corrosion Mechanisms in Wet Sour Gas Systems Containing Significant CO₂", CORROSION/96, Paper number: 96026 (Houston, Tx: NACE, 1996).
- [15] I.H. Omar, Y.M. Gunaltun, J. Kvarekval, A. Dugstad, "H₂S Corrosion of Carbon Steel Under Simulated Kashagan Field Conditions", CORROSION/2005, paper no. 05300 (Houston, TX: NACE, 2005).